

RESEARCH ARTICLE

Intracellular lipid droplets are exploited by Junín virus in a nucleoprotein-dependent process

Cecilia Alejandra Vazquez^{1,2}, Beatriz Escudero-Pérez^{3,4}, Jennifer M. Hayashi⁵, Kristoffer E. Leon⁵, João Paulo Moreira⁵, Mayra Alejandra Castañeda Cataña², Allison Groseth⁶, Melanie Ott⁵, Lisa Oestereich^{3,4}, César Muñoz-Fontela^{3,4}, Cybele Carina Garcia^{2,*} and Sandra Myriam Cordo^{1,*,‡}

ABSTRACT

Lipid droplets (LDs) are organelles involved in lipid storage, maintenance of energy homeostasis, protein sequestration, signaling events and inter-organelle interactions. Recently, LDs have been shown to favor the replication of members from different viral families, such as the Flaviviridae and Coronaviridae. In this work, we show that LDs are essential organelles for members of the Arenaviridae family. A virus-driven reduction of LD number was observed in cultures infected with Junin mammarenavirus (JUNV), caused in part by action of the viral nucleoprotein. Notably, we identified a new pool of nucleoprotein and viral RNA that localizes in the vicinity of LDs, suggesting that LDs play a role during the viral replication cycle. Regarding the mechanism behind LD exhaustion, we found evidence that lipophagy is involved in LD degradation with the resulting fatty acids being substrates of fatty acid β-oxidation, which fuels viral multiplication. This work highlights the importance of LDs during the replication cycle of JUNV, contributing to the knowledge of the metabolic changes these mammarenaviruses cause in their hosts.

KEY WORDS: Junín virus, Lassa virus, Lipid droplets, Nucleoprotein

INTRODUCTION

Lipid droplets (LDs) are cellular organelles consisting of a neutral lipid core surrounded by a monolayer of phospholipids and cholesterol. Different proteins are located on their surface, but those belonging to the perilipin family are the most prominent. Perilipin 1 (PLIN1), which is expressed in adipocytes, and perilipin 2 (PLIN2),

¹Laboratorio de Procesos Moleculares de la Interacción Virus-Célula, Departamento de Química Biológica (QB), Facultad de Ciencias Exactas y Naturales (FCEyN), Universidad de Buenos Aires (UBA)-Instituto de Química Biológica de la Facultad de Ciencias Exactas y Naturales (IQUIBICEN)-Consejo Nacional de Investigaciones Científicas y Técnicas (CONICET), Buenos Aires, C1428EHA, Argentina. ²Laboratorio de Estrategias Antivirales, Departamento de Química Biológica (QB), Facultad de Ciencias Exactas y Naturales (FCEyN), Universidad de Buenos Aires (UBA)-Instituto de Química Biológica de la Facultad de Ciencias Exactas y Naturales (IQUIBICEN)-Consejo Nacional de Investigaciones Científicas y Técnicas (CONICET), Buenos Aires, C1428EHA, Argentina. ³Bernhard Nocht Institute for Tropical Medicine, 20359 Hamburg, Germany. ⁴German Center for Infection Research (DZIF), Partner Site Hamburg-Lübeck-Borstel-Riems, 20359 Hamburg, Germany. ⁵J. David Gladstone Institutes, San Francisco, CA 94158, USA. 6Laboratory for Arenavirus Biology, Institute of Molecular Virology and Cell Biology Friedrich-Loeffler-Institut, 17493 Greifswald-Insel Riems, Germany.

© C.A.V., 0000-0002-1120-8478; B.E., 0000-0003-3655-0525; J.M.H., 0000-0001-7153-9212; K.E.L., 0000-0003-2424-0458; A.G., 0000-0001-9528-5130; M.O., 0000-0002-5697-1274; L.O., 0000-0003-0098-7485; C.M., 0000-0002-7725-2586; C.C.G., 0000-0002-6431-7176; S.M.C., 0000-0002-0652-0803

Handling Editor: Michael Way

Received 8 November 2023; Accepted 11 September 2024

which is expressed ubiquitously, are marker proteins for LDs (Itabe et al., 2017). These organelles have a central role in lipid storage and energy homeostasis but are also involved in an expanding range of cellular processes. They play important roles in signaling events, short-term protein sequestration, and inter-organelle interactions (Fujimoto and Parton, 2011). Importantly, LDs also contribute to antiviral innate immune pathways, although further comprehensive studies are required (Monson et al., 2021a,b).

LDs are also exploited by different viruses to support their replication. The *Flaviviridae* is one of the better studied viral families in relation to LDs. Hepatitis C virus (HCV) induces LD accumulation (Harris et al., 2011), and there are reports of dengue virus (DENV) and Zika virus (ZIKV) inducing both an increase (Samsa et al., 2009; Monson et al., 2021a) as well as a decrease (Jordan and Randall, 2017; García et al., 2020) in LD abundance. Given that LDs are such diverse and dynamic organelles, differences between cell lines and biphasic behaviors could explain these opposing phenotypes (Stoyanova et al., 2023). As for the mechanisms behind these changes, some flaviviruses have been shown to induce the degradation of LDs through lipolysis and manipulate their biogenesis (Zhang et al., 2017). Additionally, in the case of HCV and DENV, LDs serve as platforms for viral assembly (Iqbal et al., 2018; Samsa et al., 2009).

In addition, the replication of other virus families also has been shown to be impacted by LDs. For example, it has been shown that individual viral proteins induce LD accumulation during SARS-CoV-2 infection (Farley et al., 2022; Wang et al., 2023), whereas the pharmacological inhibition of LD formation significantly reduces its replication (Gomes Dias et al., 2020). By contrast, poliovirus exploits LDs to source the fatty acids needed for the formation of its own membranous replication structures (Viktorova et al., 2018).

Nevertheless, little is known about the importance of LDs in the replication cycle of the mammarenaviruses. Mammarenaviruses encompass those members of the Arenaviridae family that can infect mammals. Owing to their zoonotic nature, they are mostly restricted to specific geographic regions and can be controlled but not eradicated. They comprise a number of important human pathogenic viruses that cause life-threatening hemorrhagic fevers and which are classified as 'Category A Priority Pathogens' by the USA Centers for Disease Control and Prevention. Mammarenaviruses are historically classified into Old World (OW) and New World (NW) complexes depending on their serological, phylogenetic and geographical characteristics. Lymphocytic choriomeningitis and Lassa virus (LASV) are the prototypes of the OW serocomplex, whereas the non-pathogenic Tacaribe virus (TCRV) is the prototype of the NW serocomplex. LASV causes a deadly viral hemorrhagic fever, Lassa fever, and is endemic in some countries of West Africa, posting a serious health concern in these regions. By contrast, Junín virus (JUNV) belongs to the NW serocomplex and is the etiological agent

^{*}These authors contributed equally to this work

[‡]Author for correspondence (scordo@qb.fcen.uba.ar)

of Argentine hemorrhagic fever (AHF). It is endemic in Argentina and has case fatality rates of 15–20% (Enria et al., 2011). Although an effective live attenuated vaccine has been developed and is locally produced to prevent AHF in at-risk populations, and a plasma-banking system allows neutralizing antibody therapy to be performed on a limited scale within the endemic area, no specific post-exposure therapy is currently available to treat this disease. Recently, in January 2020, AHF was diagnosed in a woman in Brussels (Belgium) who had traveled from Argentina to Europe while still presenting nonspecific symptoms (Veliziotis et al., 2020). This case demonstrates the real risk of imported NW arenavirus hemorrhagic fevers outside of South America, and thus the need to have therapeutic options available for use also in non-endemic regions.

The JUNV genome consists of two single-strand RNA molecules that associate with the nucleoprotein (NP) and the viral RNA polymerase (L) to form the ribonucleoprotein complex (RNP). The viral particle also has an envelope into which the viral glycoprotein complex (comprising GP1, GP2 and SSP) is inserted. This complex is responsible for receptor binding as well as subsequent fusion during virus entry. The matrix protein (Z) is located underneath the virus envelope and drives particle morphogenesis and budding. The members of this family employ an ambisense coding strategy, with both their transcription and replication based on the activity of the viral polymerase as part of the RNP complexes. Although this process, as well as the rest of the viral life cycle, is presumed to take place in the cytoplasm of the infected cells, its specific location is still unknown (revised in Radoshitzky and de la Torre, 2019; Sepúlveda et al., 2022; Kumar et al., 2023).

In addition to viral factors, host factors, such as host proteins, metabolites and cellular energy sources, also play key roles in infection. In particular, the replication cycle of JUNV has been shown to rely on a specific cellular lipid configuration. Data from our previous studies has shown that treatments that alter general lipid metabolism diminish virus yield, suggesting an intimate relationship between viral morphogenesis and lipid availability (Cordo et al., 1999; Bartolotta et al., 2001; York and Nunberg, 2016). We, and others, have also demonstrated that cholesterolenriched membrane microdomains are involved in budding and infectious JUNV particle production (Cordo et al., 2013; Gaudin and Barteneva, 2015). Moreover, it has also been shown that replication-transcription complexes (RTCs) containing newly synthesized viral RNA are associated with cellular lipids or membranes (Baird et al., 2012). Furthermore, we have recently shown that viperin (also known as RSAD2), a cellular restriction factor that localizes on the surface of LDs, is upregulated during JUNV infection. This cellular protein also has antiviral activity against JUNV and interacts with the viral NP, suggesting that LDs might be relevant to mammarenavirus infection (Peña Cárcamo et al., 2018). Thus, the aim of this present work was to investigate the potential role of LDs during JUNV multiplication.

RESULTS

Effect of LD modulation on JUNV infection

Although all cell types contain LDs, this work was carried out in the human hepatoma cell line Huh.7, a widely used model for the study of LD physiology. Protocols for the inhibition or stimulation of LDs synthesis were implemented. Specifically, the fatty acid synthase inhibitor C75 was used to reduce cellular LD content (Loftus et al., 2000; Wang et al., 2005), whereas LD accumulation was stimulated by the addition of oleic acid (OA) (Brasaemle and Wolins, 2017). Staining for neutral lipid content with the specific fluorescent

hydrophobic probe Bodipy allowed LDs to be visualized as green spheres with a cytoplasmic distribution. In a physiological state (MEM, Fig. 1A), the size and number of LDs varies in individual cells within the same culture; however, as expected, the abundance of this organelle was effectively and clearly modulated by both treatments, consistent with previous reports (Brasaemle and Wolins, 2017; Peña Cárcamo et al., 2018). The representative phenotype of cells stimulated with OA exhibited a significant increase in both the number and size of LDs (Fig. 1A–C). By contrast, treatment with C75 led to a significant decrease in LD size (Fig. 1B), but not in abundance (Fig. 1C).

Once the experimental conditions for LD modulation in Huh.7 cells were established, cell cultures were treated with OA or C75 and infected to assess the effect of these treatments on viral replication by plaque assay and RT-PCR of viral genes n and z. Cells were infected and after 24 hours post infection (h.p.i.), both virus production and viral RNA synthesis were negatively affected in cultures with impaired LD biosynthesis (i.e. following C75 treatment), when compared to the non-treated cultures (Fig. 1D,E). Virus production was reduced by 55.4% and viral RNA levels were decreased by a comparable amount. Conversely, lipid-loaded cultures (i.e. following OA treatment) were able to produce virus titers 58.5% higher than the non-treated controls. Again here, comparable results were obtained at the level of viral RNA.

These results, indicating that LDs are important organelles that impact JUNV multiplication and viral RNA synthesis, led us to further analyze viral protein expression and localization in cultures where LD biosynthesis had been modulated. Monolayers were incubated with OA, C75 or MEM (control), infected with JUNV and then fixed at 48 h.p.i. for labeling with specific antibodies against the viral GP1, which binds to the immature, uncleaved protein as well as the mature glycoprotein (Fig. 1F) or NP (Fig. 1G). Additionally, LDs were immunolabeled using antibodies raised against PLIN2. PLIN2 belongs to the perilipin family, a group of proteins that are located on the surface of LDs, and is thus used as a bona fide marker protein for this organelle (Kimmel et al., 2010). PLIN2-labeled LDs appear as spherical (green) structures (Fig. 1F,G). Alternatively, in larger LDs, PLIN2 can be seen forming ring-like structures with unlabeled cores due to the peripheral localization of this protein. Consistent with our data optimizing the modulation of LD biosynthesis in response to chemical treatment (Fig. 1A), LDs were larger and more abundant in cultures treated with OA, and smaller when treated with C75. When inspecting the expression of the studied viral proteins, we found that in addition to the well-known cytoplasmic localization of NP (red), its staining also suggests a close apposition to PLIN2-labeled LDs (Fig. 1G, middle column) under conditions where LD biosynthesis was stimulated (i.e. OA treatment). The magnified area shown in the inset of Fig. 1G illustrates that these NP puncta can locate in close proximity to the LD core (delimited with a dotted line).

Impairment of LD biosynthesis, by treatment with C75, produced no changes in NP distribution but led to a reduced number of infected cells (Fig. 1G, right column), consistent with its negative impact on viral RNA synthesis and growth. By contrast, we observed no difference in the spatial distribution of GP1 in either stimulated or inhibited conditions when compared to the controls and, in particular, no localization or proximity to LDs was evident (Fig. 1F).

JUNV NP partially localizes in close apposition to the LD surface

Although the data in Fig. 1G suggested some small areas of colabeling of NP and PLIN2 under OA-stimulated conditions, the interpretation of this pattern as colocalization could not be

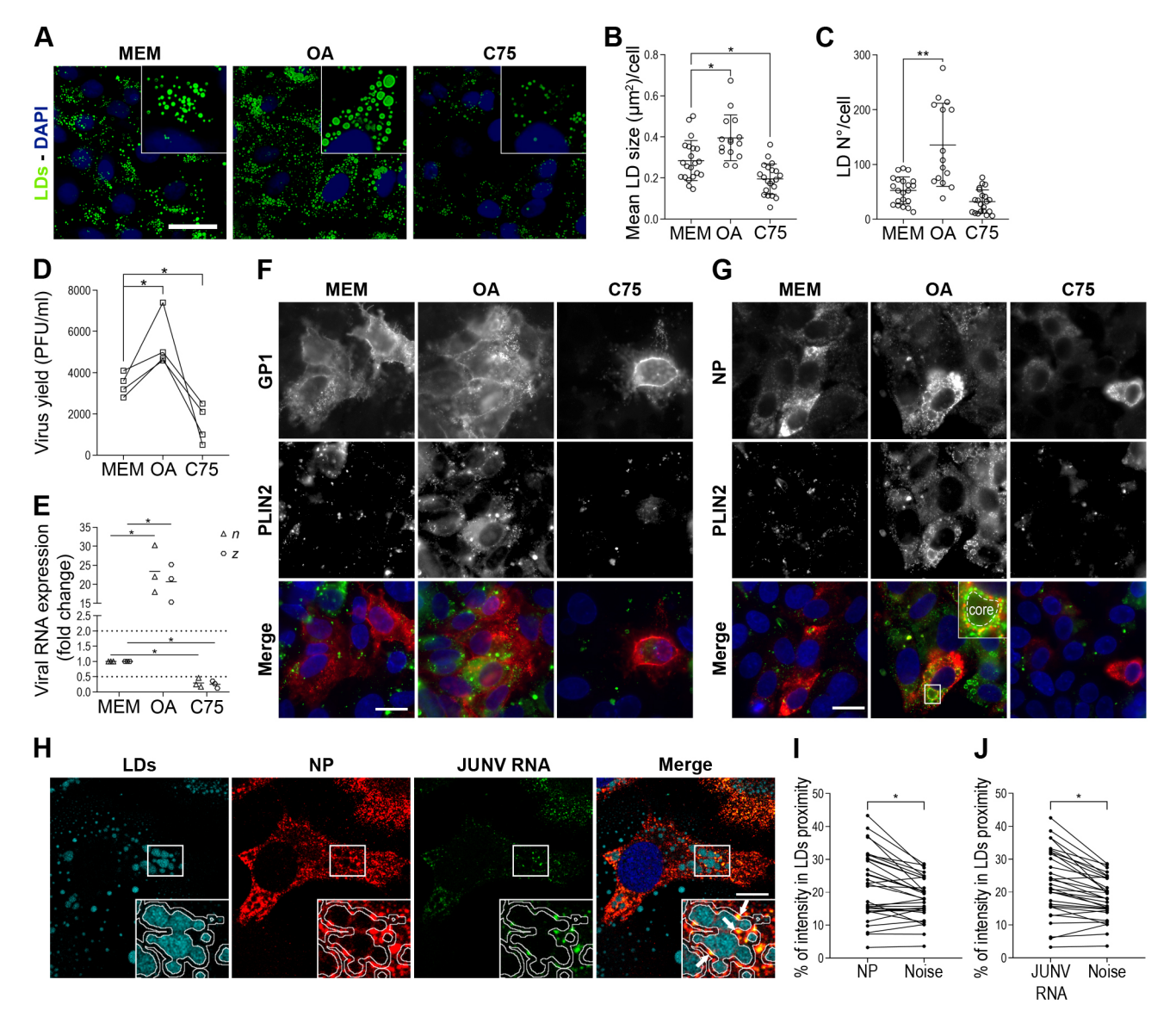


Fig. 1. Modulation of LD biosynthesis and its effect on JUNV replication. (A) Representative microscopy images of Huh.7 cells treated with OA, C75 or MEM for 24 h. LDs were labeled using the fluorescent probe Bodipy (green), and nuclei were stained with DAPI (blue). Insets show high-magnification images of LDs. Scale bar: 30 µm. (B,C) Mean LD size (B) and LD number (C) per cell measured in the cultures shown in A. Each circle represents the data of one individual cell (n=21 cells for MEM, 15 cells for OA and 21 cells for C75 treatment) where the superimposed plot shows the mean±s.d. *P<0.05; **P<0.01 (Kruskal-Wallis test for non-parametric distribution). (D) Virus yield quantified from cell supernatants of treated and untreated JUNV-infected cells at 24 h.p.i. Results from four independent experiments are shown. Data points joined by a line belong to the same experiment. *P<0.05 (one-way ANOVA followed by Dunnett's post hoc test. (E) Quantification of the viral genes n and z in treated and untreated JUNV-infected cells, relative to the housekeeping gene actin. Fold change from three independent experiments are shown, with the mean marked. *P<0.05 (one-way ANOVA followed by Dunnett's post hoc test). (F,G) Representative microscopy images of treated and untreated JUNV-infected cells at 48 h.p.i. Viral proteins, NP and GP1, were immunolabeled in red and the LDmarker protein, PLIN2 was labeled in green. Nuclei were stained with DAPI (shown in blue). Representative images from three repeats are shown in all cases. In the middle column of NP images, inset shows magnification of a LD. PLIN2 and NP can be seen on its surface, and the LD core is marked with a dotted line. Scale bars: 20 µm. (H) Association of viral components with LDs. Representative confocal images of NP and viral RNA in JUNV-infected cells. Nascent RNA, shown in green, was labeled using click chemistry; LDs (cyan) were labeled with LipidTox Deep Red; viral NP (red) was immunolabeled using specific antibodies. In the merged image, DAPI-stained nuclei are shown in blue. Inset: detail of NP and viral RNA puncta in apposition to the LD surface (arrows). ROIs corresponding to the LD surface are shown in white. Scale bar: 10 µm. (I,J) Percentage of NP (I) or viral RNA (J) that is localized on the LD surface, paired to the percentage of fluorescence of a random noise measured in the same location. Each pair of dots joined by a line represents the data of one individual cell quantified in the red channel (NP), green channel (viral RNA) and a noise image (n=32 cells). *P<0.05 (two-tailed paired t-test).

confidently asserted under these experimental conditions. Therefore, an approach using confocal microscopy was necessary to reveal the precise position of NP relative to these organelles. Moreover, taking into consideration that NP is a fundamental component of the RTCs, we also analyzed whether viral RNA is also found in the vicinity of LDs. To assess this hypothesis, nascent

viral RNA was labeled in JUNV-infected cells using click technology. Cellular RNA synthesis was inhibited starting at 46 h.p.i., after which cultures were incubated with 5-ethynyl uridine prior to fixation at 48 h.p.i., followed by click-labeling and NP immunolabeling. LDs were stained with the neutral lipid probe LipidTox. As expected, viral RNA was found in the

cytoplasm, colocalizing with NP (Fig. 1H, green and red). Also, some foci of nascent RNA and NP were found to localize in the vicinity of LDs (white arrows) but were also detected separated from these organelles. In order to determine whether this proximity to LDs was statistically significant and different from what would be expected from a randomly distributed signal, confocal images were analyzed using Fiji software (Schindelin et al., 2012). We developed an analysis algorithm whereby a ring-shaped area with a width of 0.5 µm and immediately surrounding the neutral lipid core of LDs was defined, representing the LD surface (Fig. 1H, inset, delimited in white), as well as another area comprising the whole cell. We then quantified the intensity of NP (Fig. 1H, red) and viral RNA (Fig. 1H, green) staining in both areas and calculated the percentage of each viral component localizing in the proximity of LDs, relative to its total intensity within the cell. In parallel, the same analysis was performed using the areas defined for each individual cell and its LDs, but measuring the intensity of a computer-generated image containing only noise. For each cell, the percentage of NP or viral RNA localizing next to LD core was compared to the percentage of random noise found in the same region. As shown in Fig. 1I, J, the levels of NP and JUNV's nascent RNA intensity measured in the vicinity of LDs were significantly higher than the levels of random noise.

JUNV infection and NP expression lead to a reduction in LDs

We have previously reported decreased PLIN2 expression in cells infected with JUNV at 48 h.p.i. Imaging of the infected monolayers allowed us to quantify PLIN2 punctate structures, which suggested a decrease in LDs in those cells (Peña Cárcamo et al., 2018). There are reports that in cells infected with other viruses such as DENV, PLIN2 might be displaced from LDs by viral proteins (Samsa et al., 2009). Therefore, we intended to expand our previous findings and perform comparable experiments by labeling these organelles with a lipid-sensitive probe. Huh.7 monolayers infected with JUNV were fixed at 48 h.p.i. and then incubated with anti-NP antibodies and Bodipy. Representative images are shown in Fig. 2A. Further image analysis classified cells into those expressing viral antigen (JUNV+) and those not expressing viral antigen (JUNV-) based on NP staining. Then, the number of Bodipy-labeled LDs was quantified in each individual cell. Non-infected control samples were processed in parallel and similarly analyzed. A raincloud plot shows the raw data and distribution of LD numbers per cell (Fig. 2B). LD numbers in JUNV+ cells were significantly lower compared to cells from mock-infected monolayers (51.4±19.3% decrease; mean±s.d.). Surprisingly, a similar decrease in LDs number was observed in JUNV- cells from infected monolayers. Thus, when LD abundance was analyzed with a fluorescent lipid probe, a general depletion of this organelle was seen in every cell from the infected monolayers.

In order to compare this novel result with another member of the mammarenavirus genera, a similar analysis was performed in monolayers infected with LASV. Cells were labeled, imaged and classified as for the JUNV-infected samples (Fig. 2C). Quantification of cellular LD abundance showed that LASV+cells have 300.3±54.3% more LDs than mock-infected cells. At the same time, LASV-cells in infected cultures also showed an increase in LD content of 211.7±43.5% relative to non-infected control cells. When comparing these two populations, we found that LASV+cells have 145.9±31.1% more LDs than LASV- cells from the same monolayer (Fig. 2D).

To determine whether the innate immune response is involved in the observed reduction in LDs during JUNV infection (Fig. 2A,B), we transfected cell monolayers with 10 μ g/ml poly(I:C), which

mimics dsRNA molecules. Given that transfection reagents have been reported to alter lipid homeostasis (Böttger et al., 2015), a Lipofectamine control was performed to assess its effect on LDs abundance. This control consisted of treating cells with Lipofectamine in the same way as was used for poly(I:C) transfection. Monolayers were fixed at 24 h and 48 h post transfection and then labeled with Bodipy. Representative images of cultures at 24 h post-treatment are shown (Fig. 2E). Immunolabeling of poly(I:C), shown in red, allowed us to confirm the efficiency of the treatment. We observed that LDs, labeled in green, were present in all conditions. However, their abundance was significantly higher when the interferon (IFN) response was activated by poly(I:C) treatment (Fig. 2E). Quantification showed that at 24 h the mean number of LDs in nontreated cells was 8.8±8.4 and 16.2±15.7 (mean±s.d.) in cells treated with Lipofectamine, whereas it increased to 27.2±19.3 in cells transfected with poly(I:C) (Fig. 2F). After 48 h, no difference was detected between the different conditions (data not shown). Therefore, the decrease in LDs observed during JUNV infection is not induced by the activation of the IFN pathway in response to the infection.

To further examine a possible role for viral proteins in LD depletion, we studied the effect of independently expressing different viral proteins on LD abundance. Cell monolayers were transduced with a lentiviral vector coding for either NP or Z, both fused to a FLAG tag. An empty vector was used as a control. After 48 h, transduced monolayers were fixed and labeled with an anti-FLAG antibody to detect the viral proteins and the LD lipid core was stained with LipidTox (Fig. 2G). LD abundance was quantified in individual cells expressing either protein. No differences were found between Z-expressing cells and control cells (vector); however, cells expressing viral NP showed a significant decrease in total LDs content (51.6% reduction), relative to the control (Fig. 2H). Thus, the sole expression of NP is able to induce, at least in part, the reduction of LDs observed in infected cells (Fig. 2A,B).

With regard to the decrease in LDs content observed in JUNVcells, a similar bystander effect on LDs has been previously reported for other viral models (Chen et al., 2020). This bystander effect could be caused by the transmission of cellular and viral factors from an infected cell to its neighboring cells either by intercellular channels or as soluble factors present in the culture media. We investigated the second option by harvesting the conditioned medium from cultures that had been infected for 48 h and inactivating the viral particles present in them through a brief UV light exposure. We then used this UV-inactivated conditioned medium to treat cells and quantify their LD content. As a control, the same process was carried out with medium from mock-infected cultures (Fig. 21). The lack of infectivity in UV-inactivated supernatants was corroborated by plaque assay (Fig. 2J). Quantification of both the mean Bodipy fluorescence (Fig. 2K) and the number of LDs per cell (Fig. 2L) showed that cells treated with UV-inactivated conditioned medium from infected cultures present fewer numbers of LDs than cultures treated with UV-inactivated conditioned medium from mock-infected controls. This allows us to conclude that soluble factors secreted by cells (either JUNV+ or JUNV-) to their medium are capable of inducing a reduction in LDs.

Study of lipid metabolism in JUNV-infected cells

We next approached the study of different pathways involved in LD turnover that might be regulated during JUNV infection (depicted in Fig. 3A). In particular, there have been reports that infection with other viral models induces the differential expression of lipid metabolism-related genes (Sun et al., 2013; Gomes Dias et al., 2020). We examined the expression of genes coding for proteins

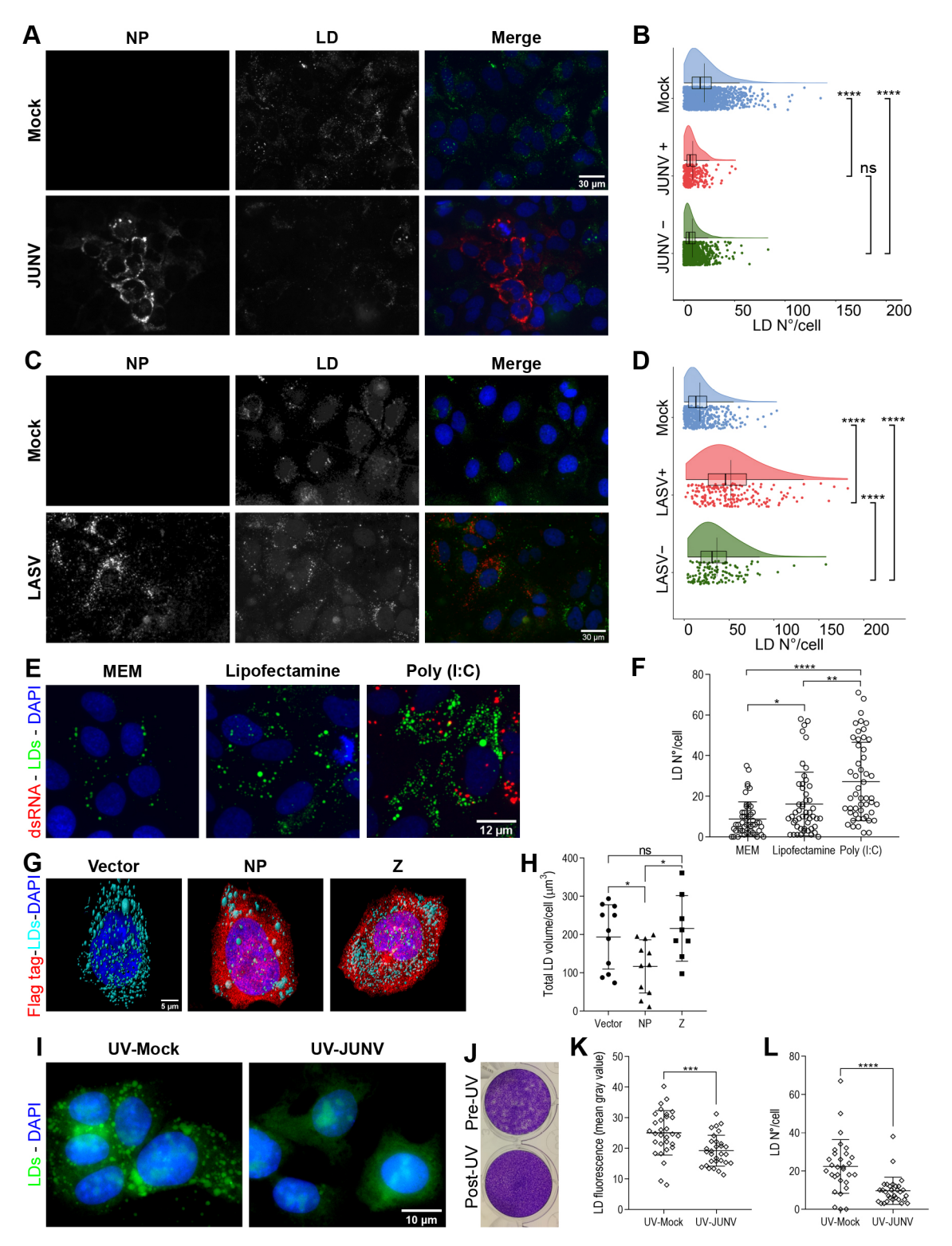


Fig. 2. See next page for legend.

relevant to LDs synthesis (FASN, DGAT1 and DGAT2), degradation (PNPLA2 and CPT1A) or coding for structural proteins (PLIN2). Monolayers were mock-infected or infected with JUNV, and at 24 h.p.i. samples were harvested as indicated in the Materials and Methods section. The expression levels of the studied genes were determined by RT-PCR and expressed as fold change (Fig. 3B). The transcription levels of the studied genes

were not significantly different between JUNV-infected and non-infected samples.

Autophagy is known to be triggered during JUNV infection where it exerts a pro-viral influence (Perez Vidakovics et al., 2019; Roldán et al., 2019). However, lipophagy, a selective type of autophagy targeted towards LDs, has not been addressed so far but could serve as a catabolic route leading to LD reduction. As an

Fig. 2. JUNV infection and NP induce a decrease of LDs.

(A) Representative microscopy images of mock-infected (upper panel) or JUNV-infected (lower panel) cells. In the merged image, viral NP has been labeled in red and LDs in green. Scale bar: 30 µm (B) Raincloud plot of the number of LDs per cell in mock-infected cultures, and cells expressing the viral antigen (JUNV+) or not (JUNV-) from infected cultures. Each dot represents the data of one individual cell (n=1575 cells for Mock, 270 cells for JUNV+ and 1308 cells for JUNV-). (C) Representative microscopy images of mockinfected (upper panel) or LASV infected (lower panel) cells. Viral NP was labeled in red and LDs in green. Scale bar: 30 µm. (D) Raincloud plot of LD number per cell in mock-infected cultures, and cells expressing the viral antigen (LASV+) or not (LASV-) from infected cultures. Each dot represents the data of one individual cell (n=464 cells for Mock, 184 cells for LASV+ and 123 cells for LASV-). In the raincloud plots in B,D, the box represents the 25-75th percentiles, and the median is indicated. The long line represents the mean. (E) Representative images of cells transfected for 24 h with poly(I:C), treated only with Lipofectamine or control cells without any treatment. LDs were stained using Bodipy (shown in green) and poly (I:C) was detected using an anti-dsRNA antibody (red). Scale bar: 12 µm. (F) Quantification of LD number per cell of the cultures shown in E. Each dot represents the data of one cell (n=50 for each treatment). (G) Representative images of cells transduced with lentiviral vectors expressing either NP or Z. A vector expressing blue-fluorescent protein was used as a control. Viral proteins were immunolabeled in red and LDs are shown in cyan. Scale bar: 5 µm. (H) Quantification of the cultures shown in G. Each dot represents the data of one individual cell (n=11 cells for the empty vector, 11 cells for NP and 8 cells for Z). (I) Representative images of cell cultures treated for 24 h with UVinactivated supernatants of mock-infected or JUNV-infected cultures. LDs. shown in green, were labeled using the fluorescent probe Bodipy. Nuclei are shown in blue. Scale bar: 10 µm. (J) Representative images of plaque assay in 16-mm diameter wells. Conditioned medium from JUNV-infected cells, before and after UV inactivation. (K) Mean fluorescence intensity in the green channel of cells treated with UV-inactivated conditioned medium, represented in I. Each data point corresponds to one cell (n=30 for each treatment). (L) Number of LDs per cell in cultures treated with UV-inactivated supernatants originated from mock- or JUNV-infected cultures. Each data point corresponds to one cell (n=30 for each treatment). (F, H, K and L) Error bars are mean±s.d. ****P<0.0001; **P<0.01; *P<0.05; ns, not significant (Kruskal-Wallis test for non-parametric distribution in B, D, F and H). ***P<0.001; ****P<0.0001 (Welch's t-test in K and L).

indicator of lipophagy, we sought to study whether lysosomes were involved in LD degradation. JUNV-infected monolayers were labeled with Lysotracker probe, fixed and JUNV+ cells were identified with anti-NP antibodies. Representative images of these samples are shown in Fig. 3C. Again, a reduction in the number of LDs was noticeable in the infected cells. In infected cells, we found several instances of colocalization between LDs and lysosomes (Fig. 3C, inset).

In order to confirm the relevance of autophagy or lipophagy in the development of this phenotype, we infected cells with JUNV and then treated them with the well-known inhibitor of autophagy, chloroquine (CQ), which decreases autophagosome–lysosome fusion (Mauthe et al., 2018). We found that in infected cultures treated with 12.5 μM CQ, the levels of LDs were completely restored and even surpassed those from mock-infected cultures (Fig. 3D,E). Also, as expected, treatment with CQ reduced viral titers by one order of magnitude (data not shown). In conclusion, autophagy, and in particular lipophagy, are mechanisms that lead to the reduction of LDs in JUNV-infected cells, although the participation of other pathways should still be investigated.

LD degradation leads to the release of free fatty acids. The primary pathway for their catabolism is fatty acid β -oxidation (FAO) (Kloska et al., 2020), which has been described as being important in the replication of other viruses (Heaton and Randall, 2010; Manokaran et al., 2020; Zheng et al., 2022). To assess whether FAO is necessary for JUNV replication, cell monolayers were infected

and treated with etomoxir (ETO), an irreversible inhibitor of this pathway (Ceccarelli et al., 2011). Supernatants were harvested at 48 h.p.i. and cells were either harvested for RNA isolation or fixed for immunolabeling. We observed that without a relevant effect on cell viability (Fig. 4A), treatment with 50 µM ETO reduced viral RNA levels by 82% (Fig. 4B) and viral yield by up to 97% (Fig. 4C), indicating that FAO is necessary for efficient virus multiplication. However, when LD content was analyzed via immunofluorescence microscopy, we found that ETO treatment did not prevent the reduction in LD number in JUNV-infected cells, thus excluding a direct role of FAO on the generation of this phenotype (Fig. 4D,E).

DISCUSSION

Cellular lipid metabolism, organization and availability are highly relevant in the context of viral infections. Particularly, the importance of cholesterol has been widely studied in the replication cycle of JUNV. Previous studies from our group have shown that cholesterol availability in infected cells is crucial for proper JUNV replication. An inhibitor of the 3-hydroxy-3-methylglutaryl-CoA (HMG-CoA) reductase, lovastatin, inhibits the biosynthesis of cholesterol and has antiviral activity against JUNV. We further demonstrated that the resulting cholesterol depletion modified the cell cholesterol-enriched membrane domains and, in turn, the fate of the JUNV glycoprotein complex, thus impairing normal viral morphogenesis (Cordo et al., 2013). Moreover, due to their enhanced lipophilicity, oxysterols (naturally occurring cholesterol derivatives) can be incorporated into cell membranes, altering their physical properties and indirectly affecting membrane proteins (Rentero et al., 2008; Olkkonen and Hynynen, 2009). We have also demonstrated that cell media supplementation with oxysterols has a detrimental effect on the plasma membrane localization of JUNV GP1 (Cordo et al., 2013). In addition to the cell plasma membrane and cholesterol-enriched domains, cholesterol is stored in intracellular LDs in the form of cholesterol esters, and these lipidic structures have been shown to be key for the replication of several viruses. For instance, atorvastatin, another reversible inhibitor of HMG-CoA reductase, downregulates cholesterol, reduces the formation of LDs and impairs the replication of ZIKV (Stoyanova et al., 2023) and influenza A virus (Episcopio et al., 2019). LDs are organelles with a continuously growing list of functions. They serve as intracellular sites for neutral lipid storage and are crucial for lipid metabolism and energy homeostasis. As previously mentioned, LDs have also been described to play key roles in the propagation of several infectious agents. There is evidence that these organelles act as assembly and replication platforms for specific viruses, whereas others exploit their contents as an energy source (Samsa et al., 2009; Cheung et al., 2010; Viktorova et al., 2018; Cloherty et al., 2020). At the same time, LDs also form part of the immune response, acting as reservoirs for proteins that counteract intracellular pathogens and act as hubs for the production of inflammatory mediators (Monson et al., 2021b).

In this work, we investigated the relevance of LDs during JUNV infection. Our results showed that the inhibition of cellular LD synthesis hinders viral multiplication, whereas the stimulation of LD accumulation leads to an increase in viral replication. This finding indicates that LDs are necessary to maintain viral replication. Detailed analysis and quantification of the number of LDs per cell allowed us to describe a novel phenotype whereby LD abundance is reduced in infected monolayers compared with the number seen in mock-infected monolayers. Monson et al. have described that the activation of the innate immune response in primary astrocytes induces LD accumulation (Monson et al., 2021a). Likewise,

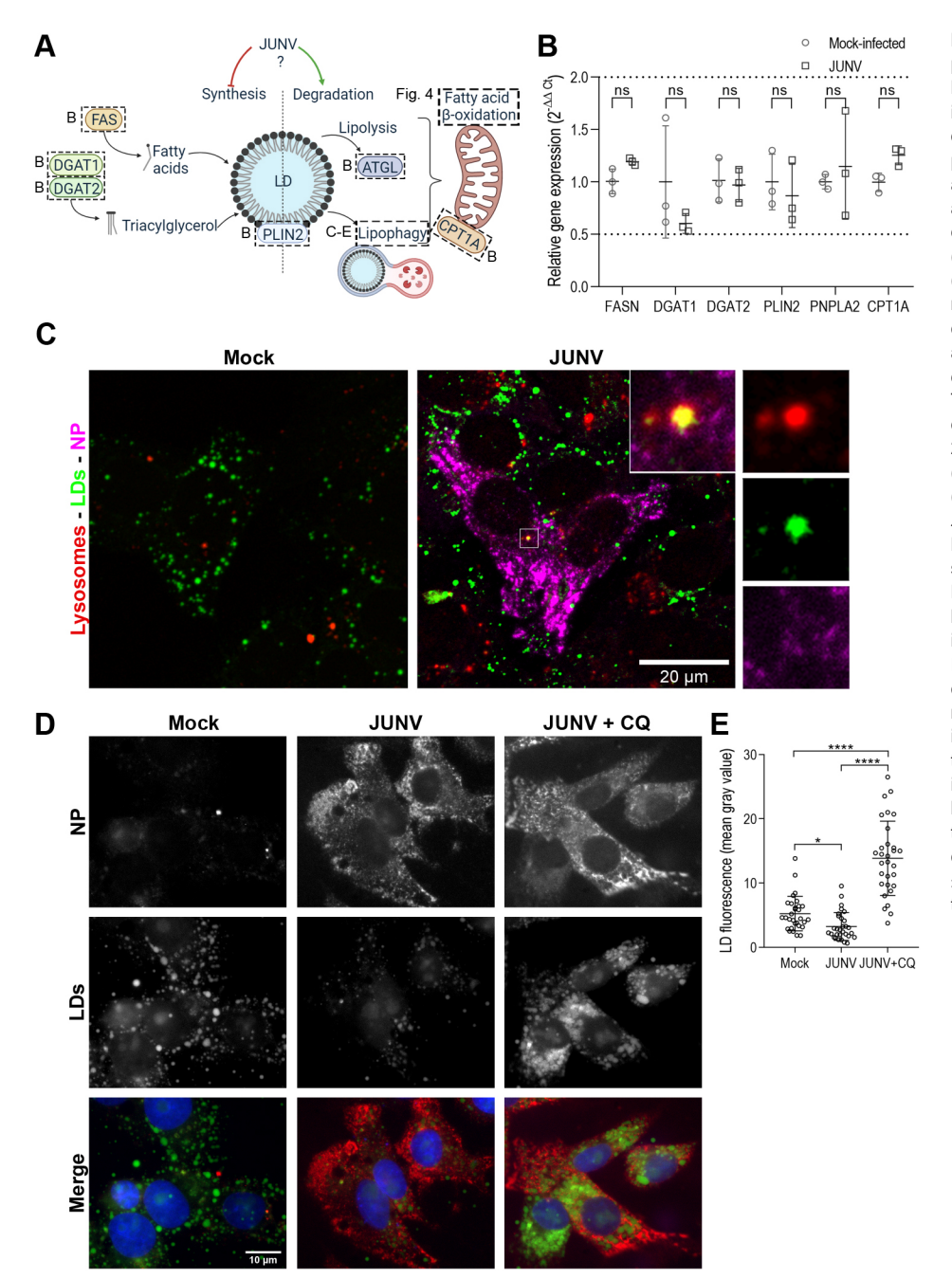


Fig. 3. Involvement of different metabolic pathways in JUNV-induced reduction of LDs. (A) Diagram of pathways and key genes involved both in LD synthesis and degradation. The factors addressed in the present work are enclosed with a dotted line and the panels in which each of these factors are studied are indicated in bold. (B) Relative expression of genes with roles in LD synthesis (FASN, DGAT1 and DGAT2), degradation (PNPLA2 and CPT1A) or encoding LD resident protein (PLIN2). Expression was calculated relative to the housekeeping gene actin. Individual values of three independent experiments and mean±s.d. are plotted. Thresholds for significant changes in expression (increase or reduction) were set at 2 and 0.5, respectively. ns, not significant (two-tailed unpaired Student's t-test). (C) Maximum intensity projection images of a z-stack from mock- or JUNV-infected cultures. Lysosomes and LD were labeled with the specific probes LysoTracker and LipidTox Deep Red to analyze the colocalization between these organelles. NP (magenta) was immunolabeled to identify infected cells. Inset: detail of an event of LD-lysosome colocalization. Images representative of two repeats. Scale bar: 20 µm. (D) Representative images of mock and JUNV-infected cells treated with or without CQ. NP was immunolabeled in red and LDs in green. Scale bar: 10 µm. (E) Mean fluorescence intensity in the green channel of cells shown in D (n=30 cells for each condition; error bars are mean ±s.d.). *P<0.05: ****P<0.0001 (Kruskal-Wallis test for non-parametric distribution).

Lipofectamine or poly(I:C) stimulus resulted in a transient increase of LD abundance in our model. This allowed us to discard the possibility that the activation of the IFN pathway in response to the infection accounts for the observed reduction of LDs in JUNV-infected cells. Additionally, the independent expression of NP but not Z independently induced a two-fold decrease in total LD content. Other viral proteins have been shown to be able to induce changes in cellular lipid metabolism, leading to changes in LD abundance. For example, individual SARS-CoV-2 proteins indirectly induce the accumulation of LDs (Farley et al., 2022) through an upregulation of the pathways involved in lipid uptake and triacylglycerol synthesis (Gomes Dias et al., 2020), and the inhibition of autophagic flux (Wang et al., 2023). Nonetheless, an additional contribution to this general LD decrease of other viral or cellular factors that were not analyzed in this study, cannot be

excluded. Together, our results indicate that the reduction of LDs seen in infected cultures is mediated by JUNV viral factors.

Furthermore, in the infected cultures, both JUNV antigenpositive (JUNV+) and antigen-negative (JUNV-) cells presented a similarly reduced number of LDs. It is important to consider that one limitation of this quantification method (IFA) is that early JUNV-infected cells, that are not yet antigenically positive at the time of sample analysis, are not considered. Therefore, infected cells that are not positive for NP cannot be discarded. However, these underseen cells might express biologically relevant amounts of viral protein that are sufficient to produce the observed phenotype.

The observed reduction in the number of LDs in JUNV- cells could be explained by a bystander effect in the vicinity of infected cells, such as the one described for ZIKV; Chen et al. (2020) and Stoyanova et al. (2023) have reported an upregulation of the

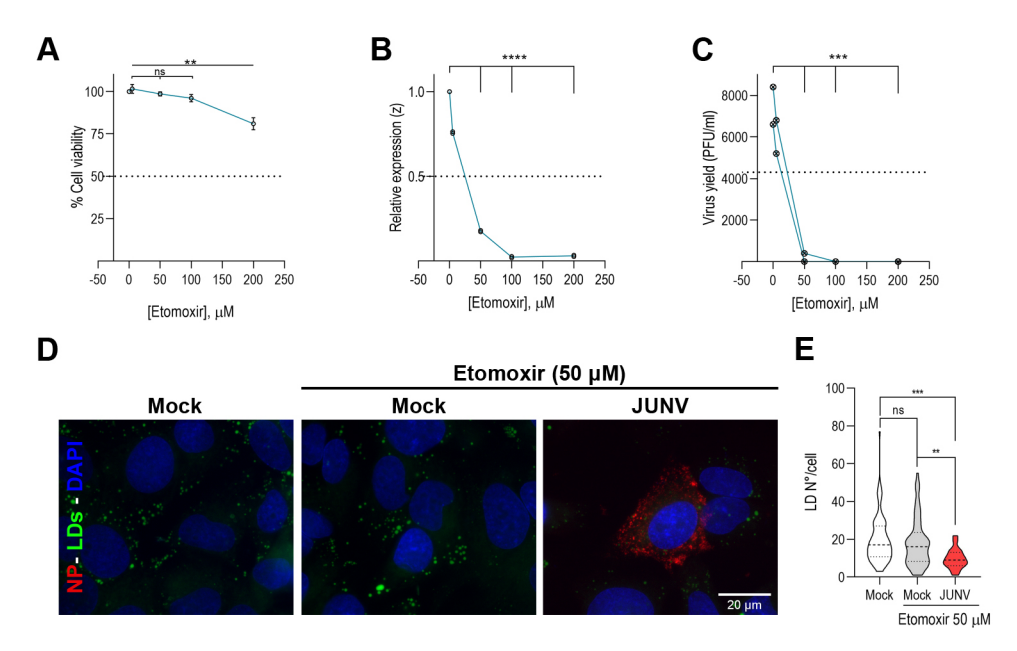


Fig. 4. Effect of ETO, an inhibitor of fatty acid beta oxidation, on JUNV multiplication and LD usage. (A) Effect of ETO on cell viability, measured with Alamar Blue assay (mean±s.d.; *n*=3). (B) Effect of ETO on viral RNA levels. Quantification of viral RNA in cell monolayers infected with JUNV and treated with different concentrations of ETO. *Z* RNA levels were determined by RT-PCR and normalized to cellular actin. Expression values are relative to non-treated controls. Data represents values of two independent replicates and the threshold for significant expression reduction was 0.5 (C) Effect of ETO treatment on JUNV yield at 48 h.p.i. Plotted data from the same experiment are connected with a line (*n*=2). (D) Representative microscopy images of JUNV-infected or mock-infected cell cultures, treated or not with ETO. LDs were stained in green with Bodipy, viral NP was immunolabeled in red, and nuclei are shown in blue. Scale bar: 20 μm. (E) Effect of FAO inhibition on JUNV-induced reduction of LDs. Violin plot shows distribution of LD number per cell (*n*=90 cells for Mock without ETO, 80 cells for Mock with ETO, 19 cells for JUNV+ with ETO). Dashed lines indicate the median and first and third quartiles.

*****P≤0.0001; ****P<0.001; ***P<0.001; ns, not significant (one-way ANOVA followed by Dunnett's post-hoc test; A, C, E)

abundance of LDs in both ZIKV+ and ZIKV- cells at 48 h.p.i. In this case, treatment of placental cultures with UV-irradiated conditioned medium harvested from ZIKV-infected cells leads to an increase in LD content, thus showing that the bystander effect can be mediated by extracellular vesicles or soluble factors in a paracrine way (Chen et al., 2020). In the case of JUNV, treatment with UV-inactivated conditioned medium also reproduced the phenotype of LD number reduction observed in JUNV- cells. Therefore, it is evident that either JUNV+ or JUNV- cells secrete soluble factors that signal towards this reduction. Finally, the exchange of viral and cellular factors between cells through gap junctions could also be contributing to this effect.

In contrast to our findings with JUNV, when analyzing infection with the OW mammarenavirus LASV, we showed an upregulation of LD abundance at 48 h.p.i. in both LASV+ and LASV- cells compared to mock-infected controls. Furthermore, LD content was higher in LASV+ than in LASV – cells. Given that LASV NP and Z protein can inhibit the IFN-I pathway (Murphy and Ly, 2022), the increase in LD abundance is likely not related to the activation of this pathway and the mechanism behind this phenotype is yet to be elucidated. These results further show that our quantification protocol is robust enough to detect LD changes in discrete cell populations. It also establishes that, in this aspect of their biology, these two important hemorrhagic mammarenaviruses behave differently, inversely modulating cellular physiology in infected cells and probably their non-infected neighbors. The relationship between this observation and the pathogenesis of these viruses remains to be studied.

As previously discussed, NP expression is sufficient to produce a decrease in LDs. Furthermore, the analysis of JUNV-infected cells showed a specific pool of viral NP localizing in close proximity to LDs. Apart from the canonical functions of NP in the replication

cycle, several other accessory roles related to pathogenesis have been described. Among these, it has been shown that NP is capable of inhibiting the IFN-I-mediated response (Shao et al., 2018) and apoptosis of infected cells (Wolff et al., 2013). Taking into consideration the multifunctionality of NP, our results provide a possible mechanism that could underlie the compartmentalization of one (or more) of these functions, or even a new function that is specifically targeted to LDs. This is particularly important for the Arenaviridae family given that no detailed data has been published regarding NP localization beyond its diffuse distribution within the cytoplasm. Even though the RTCs of JUNV and TCRV have been described to localize in low-density detergent-sensitive structures, they have not been found to colocalize with any of the organelles forming the endomembrane system (Baird et al., 2012). The albeit partial apposition between NP, viral RNA and LDs supports the notion that LDs might have a scaffolding role during the life cycle of JUNV. Additional studies will elucidate the mechanisms behind this phenotype.

JUNV RNA and NP localization in the context of LD decrease is yet another example of the complex interplay between virus and their host cells. For example, HCV is well described to induce LD accumulation, translocate several of its proteins onto the surface of LDs and use them for production of infectious progeny. By contrast, it has recently been found that the cellular colipase ABHD5 is a proviral factor associated with LDs and crucial for HCV assembly and morphogenesis (Vieyres et al., 2020). Then, HCV production also correlates with lipid droplet lipolysis and mobilization of fatty acids for morphogenesis. This could also be the case for JUNV, activating LD degradation to provide lipid components (i.e. cholesterol) necessary for membrane budding and assembly.

Different pathways can be involved in virus-driven metabolic reprogramming. For example, lipogenesis pathways are upregulated in

ZIKV-infected neural stem cells (NSCs), whereas the lipolysis factors PNPLA2 and LIPE are downregulated (Gomes Dias et al., 2023). Many Flaviviruses have also been described to induce lipophagy, leading to a decrease in LD abundance (Zhang et al., 2018). In the case of SARS-CoV-2, the expression of ORF3a induces LD accumulation by inhibiting the fusion between autophagosomes and lysosomes, thus establishing an incomplete autophagy status in cells (Qu et al., 2021). In the case of this present work, we evaluated the expression of genes coding for important metabolism-related proteins, an analysis that has not been done before for members of this family. Our results showed that, at a population level, none of the analyzed genes are transcriptionally affected by JUNV infection. Although not significant, a trend towards a decrease in DGAT1 and an increase in CPT1 and FASN expression was seen. One limitation of this analysis is that gene expression levels do not represent individual cell phenotypes but rather the combination of assorted (infected and non-infected) group of cells. Recently, a negative correlation in the activity of DGAT1 and CPT1A expression has been reported in a model of induced sepsis; pharmacological inhibition of DGAT1 prevented LD accumulation with an augment of CPT1A (Teixeira et al., 2024). In the context of JUNV infection, a viral factor could be hindering DGAT1 as a part of other factors involved in LD decrease. Therefore, the trend observed for these genes might be considered in future work.

Taking into consideration that autophagy is induced by JUNV (Perez Vidakovics et al., 2019; Roldán et al., 2019), lipophagy might represent another route of JUNV-driven LD exhaustion. Lipophagy is a type of selective autophagy that targets LDs. It begins with the recognition of LD cargo by the autophagosome through interaction with LC3-I (Singh and Cuervo, 2012). Then, the LDloaded autophagosomes mature through fusion with the lysosome, promoting the degradation of its cargo content by lysosomal acid proteases and lipases. In hepatocytes, the direct engulfment of entire LDs by lysosomes has also been described (Schulze et al., 2020). In our study, colocalization events found between lysosomes and LDs indicate that lipophagy, a highly dynamic process, could be contributing to the decrease in LD number during JUNV infection. We addressed this further by inhibiting the fusion of autophagosomes and lysosomes with CQ. Treatment with this autophagy inhibitor effectively reverted the reduction in LDs induced by infection, thus demonstrating that autophagy, and in particular lipophagy, play a direct role in the generation of this phenotype. Finally, we studied a possible function for the degradation of LDs and release of free fatty acids – energy production via FAO. We proved that this metabolic pathway is necessary for JUNV replication, consistent with the antiviral activity of ETO against JUNV.

At present, the importance of cellular lipid structures in cellular functions, as well as in the multiplication cycles of many infectious agents and viruses, is being reevaluated. In this work, we presented novel results into this field, which was previously unexplored for the *Arenaviridae* family. We demonstrated opposing modulation of LDs in response to JUNV and LASV, two major pathogenic arenaviruses. In the case of JUNV, this phenotype is triggered by the sole expression of viral NP and does not involve the modulation of master genes associated with the regulation of LD biogenesis or degradation. Also, we found that soluble factors produced by infected cultures are capable of reproducing this phenotype. We demonstrate that blockage of lysosomal-dependent lypophagy prevented LD decrease whereas inhibition of FAO did not. Therefore, in our conditions, we established that lipophagy is directly responsible for this decrease. More studies are still needed

to help unravel the role of these organelles in the different steps of the multiplication cycle of arenaviruses, and the interaction between cellular and viral factors located in their vicinity. For the first time, this study showcases LDs and their metabolism as potential targets for the development of an antiviral strategy against AHF.

MATERIALS AND METHODS

Cell lines and viruses

The human hepatocellular carcinoma cell line Huh.7 (Pablo J. Schwarzbaum, Instituto de Química y Fisicoquímica Biológicas, Facultad de Farmacia y Bioquímica, Universidad de Buenos Aires, Buenos Aires, Argentina) and African green monkey Vero cell line (ATCC, CCL-81) were grown in minimum essential medium (MEM, GIBCO) supplemented with 10% fetal bovine serum (FBS, Sigma) and $25\,\mu\text{g/ml}$ gentamicin (Sigma-Aldrich, G1397). All cell lines were authenticated and tested for contamination.

Virus stocks of JUNV attenuated IV4454 strain [Instituto Nacional de Enfermedades Virales Humanas 'Dr. Julio I. Maiztegui' (INEVH), Buenos Aires, Argentina] or pathogenic XJ strain and LASV Bantou 366 strain, lineage IV (Bernhard Nocht Institute for Tropical Medicine, Hamburg, Germany) were prepared in Vero cells and titrated using a standard plaque assay (JUNV) or immune focus assay (LASV).

LD modulation with OA and C75

Lipid loading was carried out according to the method described by Brasaemle and Wolins (Brasaemle and Wolins, 2017). Briefly, OA was mixed into a 14% bovine serum albumin (BSA) solution in 0.1 M Tris-HCl pH 8.0, in order to generate OA-BSA complexes in a 6:1 molar ratio. This solution was used to supplement the culture medium with 400 μM of OA, which was added to cell cultures 4 h prior to infection.

LD depletion was accomplished by treatment with 23 μM C75 (Sigma), which was added to cell cultures after viral adsorption and remained present until samples were harvested.

Real-time RT-PCR

Cells were seeded in six-well plates and infected with a multiplicity of infection (MOI) of 0.1 after 24 h. At the indicated time points, cells were harvested using Tri Reagent (Molecular Research Center) and RNA was isolated following the manufacturer's instructions. cDNA synthesis was carried out using Moloney murine leukemia virus reverse transcriptase (M-MLV, Promega) and random hexamer primers (Genbiotech). Real-time PCR was conducted using FastStart Universal SYBR Green Master (Rox) (Roche), according to the following protocol: 95°C for 10 min, followed by 45 cycles of 30 s at 95°C, 1 min at 60°C, and 1 min at 72°C, and a final step of 10 min at 72°C. Amplification plots were analyzed with Bio-Rad software and the comparative threshold cycle method was used to determine gene expression relative to the β -actin cellular gene. Mean fold changes lower than 0.5 or higher than 2 were respectively considered as a significant decrease or increase in gene expression. Primers used for the indicated genes and the corresponding proteins are indicated in Table S1.

Immunofluorescence assay

At the indicated time post infection, post poly(I:C) transfection with Lipofectamine, or post transduction cultures grown on glass coverslips were fixed with 4% paraformaldehyde for 10 min when working with JUNV, strain IV4454, or 4% formaldehyde for 60 min when working with the LASV or XJ strain of JUNV. Then, samples were permeabilized with 0.1% Triton X-100 in phosphate-buffered saline (PBS) for 10 min. Cells were then incubated for 1 h with a 1:300 dilution of primary antibody, followed by a 1 h incubation with a 1:300 dilution of secondary antibody. When indicated, samples were also incubated for 30 min with a 1:500 dilution of Bodipy 493/503 (Thermo Fisher Scientific, D3922) or a 1:250 dilution of HCS LipidTOX Deep Red Neutral Lipid Stain (H34477, Thermo Fisher Scientific). Finally, nuclei were stained with DAPI for 5 min (1 μ g/ml, Sigma) and samples were mounted using a glycerol mounting medium with Dabco. The entire protocol was carried out at room temperature. Samples were washed three times with PBS after every step, and once with water before mounting. The antibodies used were as follows:

rabbit polyclonal anti-Plin2 (Abcam, Ab52355), mouse monoclonal anti-JUNV NP (BEI, SA02-BG12), mouse monoclonal anti-JUNV GP1 (BEI, GB03BE08), recombinant rabbit monoclonal anti-dsRNA (J2) (Absolute antibody, Ab01299), goat anti-rabbit-IgG-Alexa 488 (Thermo Fisher Scientific, A-11008), goat anti-mouse IgG-Alexa 568 (ThermoFisher, A-11004).

For lysosome staining, cell cultures were incubated at 37°C with a 1:13,000 dilution of LysoTracker (Thermo Fisher Scientific) in culture medium for 30 min prior to fixation. Then, the immunofluorescence protocol was followed as described above. Samples were imaged in either an Olympus BX51 fluorescence microscope, an Olympus FV300 confocal microscope or a Zeiss LSM880 super resolution microscope with Airyscan.

LD number and size quantification

Image analysis was performed using the Fiji distribution of ImageJ (Schindelin et al., 2012). To establish the regions of interest (ROIs) corresponding to each individual cell, the channel corresponding to the nuclear stain was used. First, a Gaussian blur filter with a radius of 10 pixels was applied. The resulting image was processed using the 'Find maxima' plugin, whereby each nucleus was selected and the segmented particles corresponding to individual cells were obtained. These particles were analyzed and indexed as ROIs. Then, the channel corresponding to the LD stain was processed using a Gaussian blur filter with a radius of 1 pixel. Individual LDs were selected using the 'Find maxima' plugin and a binary mask where each LDs was represented as one dot was generated. Finally, the number of LDs per cell was obtained by counting the number of LD-representing dots in each of the previously defined ROIs.

In order to analyze the size of individual LDs, the channel corresponding to this organelle was smoothed with a Gaussian blur filter of 1 pixel. Then, images were thresholded and the resulting binary mask was refined using a watershed algorithm to detect boundaries between neighboring objects. Finally, we used the 'Analyze Particles' command to select objects with a circularity between 0.75 and 1.0 and measured their area.

Quantification of protein or viral RNA association with the LD surface

To quantify the association of NP and viral RNA with the surface of LDs, z-stacks of infected cells were acquired in a Zeiss LSM980 confocal microscope. We first worked with the NP channel to obtain a binary mask corresponding to the whole cell. A large radius Gaussian blur filter was applied to the NP channel and then, the z-stack was segmented using the mean gray value as the threshold. Secondly, a binary mask selecting the area immediately adjacent to the LD surface was generated. To do so, the channel with the LD neutral core signal was processed using the Gaussian blur filter to remove noise and was segmented through thresholding. The resulting binary mask was duplicated, dilated 0.5 µm (diameter of one PLIN2 puncta), and then the initial binary mask was subtracted from the dilated one to obtain a binary mask of solely the LD surface. The Analyze Particles plugin was used to obtain ROIs defined by the previously mentioned binary masks. As a control, images containing noise were generated. NP, viral RNA and noise intensity were quantified in the previously defined ROIs (in the whole cytoplasm as well as on the LD surface). The ratio between the intensity found on the LD surface and the whole cell was calculated and each pair of data (NP versus noise, or viral RNA versus noise) was compared.

Nascent RNA labeling

Huh.7 cultures were plated in 24-well plates containing coverslips at a seeding density of 5×10^4 cells per well. After 24 h cells were infected with JUNV at an MOI of 0.1. At 20 h.p.i., the medium was replaced with 300 µl of DMEM (Gibco, 12100-046) containing 20 µg/ml of actinomycin D (Sigma-Aldrich, A9415) and cells were incubated at 37°C for 30 min to inhibit cellular RNA polymerases. Then, 300 µl of DMEM containing 2 mM ethynyl uridine (Invitrogen, E10345) was added to each well and cultures were incubated for 3 h at 37°C. Samples were fixed for 30 min and immunostaining was performed as described above. After staining, the click reaction was carried out using the Click-iT RNA Alexa Fluor 488 imaging kit following the manufacturer's instructions (Thermo Fisher Scientific, C10329) and samples were mounted and imaged.

UV-inactivated conditioned medium

Huh.7 cells were plated in 24-well plates and infected with JUNV or mock infected. At 48 h.p.i., the conditioned medium was harvested, placed in an open glass Petri dish forming a thin layer and immediately UV-irradiated for 2 min using a Germicidal 15W G15T8 GL-15 lamp at a distance of 10 cm. The conditioned medium was collected and used to treat cell cultures that had been seeded on coverslips 24 h prior.

Inactivation of viral particles was confirmed by plaque assay.

Etomoxir inhibitor assays

Cell viability in the presence of ETO (Sigma-Aldrich, E1905) was determined using the alamarBlueTM Cell Viability Reagent (Invitrogen, DAL1025) as described by the manufacturer. Briefly, Huh.7 cells were grown in 96-well plates for 24 h and treated with ETO in concentrations ranging from 0 to 200 μM . Medium with ETO was replenished once after 24 h. After 48 h of treatment, 90 μl of medium was kept in each well and 10 μl of Alamar Blue reagent was added. Cultures were incubated at 37°C for 2 h and fluorescence was measured at 560 and 590 nm in a Polarstar Omega B.M.G-Plate reader.

To evaluate the effect of ETO on JUNV replication, cells were infected at an MOI of 0.1, and treated with ETO at the same concentrations as above. At 24 h.p.i., the medium was removed and replenished with fresh medium and the same concentration of ETO. At 48 h.p.i. supernatants were harvested and quantified by plaque assay. The remaining infectivity, as a percentage relative to a control without ETO, was determined.

CQ treatment

Cell cultures grown on coverslips were infected with JUNV with an MOI of 0.1. The inoculum was discarded, fresh medium was added, and cultures were incubated at 37°C for 2 h. Then, the medium was replaced by fresh medium containing CQ diphosphate salt (Sigma-Aldrich, C6628) 12.5 μ M. Cells were fixed at 48 h.p.i. and stained for microscopy analysis.

Statistical analysis and data visualization

Statistical analyses were performed using GraphPad Prism 8.0 (GraphPad Software, Inc.). Results are presented as means±s.d. When comparing two means, a two-tailed Student's *t*-test was performed. All tests were unpaired, unless otherwise specified. When necessary, Welch's correction (Welch's *t*-test) was applied. When comparing more than two means, normal distribution and homocedasticity was tested. If these assumptions were met, a one-way ANOVA test was carried out and a post-hoc Dunnett test was performed. If these assumptions were not met, a Kruskal–Wallis test was carried out. In both cases, *P*<0.05 was the criteria taken for considering differences to be significant.

Bar and violin plots were graphed using Prism 8.0 (GraphPad Software, Inc.). Raincloud plots (Allen et al., 2021) were plotted in the online app https://gabrifc.shinyapps.io/raincloudplots/.

Acknowledgements

The authors are very grateful for the excellent technical advice provided by Tim Gilberger and Roland Thuenauer. The authors would also like to acknowledge the Centro de Microscopía de Fluorescencia Gregorio Weber for use of the Zeiss LSM980 confocal microscope and Victoria Repetto for helpful discussions on data acquisition.

Competing interests

The authors declare no competing or financial interests.

Author contributions

Conceptualization: C.A.V., C.C.G., S.M.C.; Methodology: C.A.V., J.M.H., K.E.L., J.P.M., M.A.C.C.; Formal analysis: C.A.V., C.C.G., S.M.C.; Investigation: C.A.V., B.E.-P.; Resources: A.G., M.O., L.O., C.M.-F.; Writing - original draft: S.M.C.; Writing - review & editing: C.A.V., B.E.-P., J.M.H., A.G., M.O., L.O., C.M.-F., C.C.G., S.M.C.; Visualization: C.A.V.; Supervision: C.C.G., S.M.C.; Funding acquisition: C.C.G., S.M.C.

Funding

This work was funded by the Universidad de Buenos Aires under grant UBACyT 2020-2022 (S.C.); by Agencia Nacional de Promoción Científica y Tecnológica

under grants PICT-2021-0138 (S.C.) and PICT-2021-1316 (C.G.) and by Consejo Nacional de Investigaciones Científicas y Técnicas under grant PIP 11220210100168CO (C.G.). L.O. received funding from the Leibniz Association, grant no. J59/18. A.G. received intramural funding by the Friedrich-Loeffler-Institut. The collaboration with C.M.-F. laboratory in Germany was supported by a The Company of Biologists travel grant and an ISAR Chu Family Foundation Scholarships for Early Career Women in Science. The collaboration with M.O. laboratory in USA was supported by the Fulbright Commission under a Fulbright-Ministry of Education scholarships.

Data availability

All relevant data can be found within the article and its supplementary information.

First Person

This article has an associated First Person interview with the first author of the paper.

References

- Allen, M., Poggiali, D., Whitaker, K., Marshall, T. R., Van Langen, J. and Kievit, R. A. (2021). Raincloud plots: a multi-platform tool for robust data visualization. Wellcome Open Res. 4, 63. doi:10.12688/wellcomeopenres.15191.1
- Baird, N. L., York, J. and Nunberg, J. H. (2012). Arenavirus infection induces discrete cytosolic structures for RNA replication. J. Virol. 86, 11301-11310. doi:10. 1128/jvi.01635-12
- Bartolotta, S., García, C. C., Candurra, N. A. and Damonte, E. B. (2001). Effect of fatty acids on arenavirus replication: Inhibition of virus production by lauric acid. *Arch. Virol.* 146, 777-790. doi:10.1007/s007050170146
- Böttger, J., Arnold, K., Thiel, C., Rennert, C., Aleithe, S., Hofmann, U., Vlaic, S., Sales, S., Shevchenko, A. and Matz-Soja, M. (2015). RNAi in murine hepatocytes: the agony of choice—a study of the influence of lipid-based transfection reagents on hepatocyte metabolism. *Arch. Toxicol.* **89**, 1579-1588. doi:10.1007/s00204-015-1571-0
- Brasaemle, D. L. and Wolins, N. E., (2017). Isolation of lipid droplets from cells by density gradient centrifugation. *Curr. Protoc. Cell Biol.* **72**, 3.15.1-3.15.13. doi:10.1002/cpcb.10.lsolation
- Ceccarelli, S., Chomienne, O., Gubler, M. and Arduini, A. (2011). Carnitine palmitoyltransferase (CPT) modulators: a medicinal chemistry perspective on 35 years of research. *J. Med. Chem.* **54**, 3109-3152. doi:10.1021/jm100809g
- Chen, Q., Gouilly, J., Ferrat, Y. J., Espino, A., Glaziou, Q., Cartron, G., Costa, H. E., Al-Daccak, R. and Jabrane-Ferat, N. (2020). Metabolic reprogramming by Zika virus provokes inflammation in human placenta. *Nat. Commun.* 11, 2967. doi:10.1038/s41467-020-16754-z
- Cheung, W., Gill, M., Esposito, A., Kaminski, C. F., Courousse, N., Chwetzoff, S., Trugnan, G., Keshavan, N., Lever, A. and Desselberg, U. (2010). Rotaviruses associate with cellular lipid droplet components to replicate in viroplasms, and compounds disrupting or blocking lipid droplets inhibit viroplasm formation and viral replication. *J. Virol.* 84, 6782-6798. doi:10.1128/jvi.01757-09
- Cloherty, A. P. M., Olmstead, A. D., Ribeiro, C. M. S. and Jean, F. (2020). Hijacking of lipid droplets by hepatitis C, dengue and zika viruses-from viral protein moonlighting to extracellular release. *Int. J. Mol. Sci.* 21, 7901. doi:10.3390/ijms21217901
- Cordo, S. M., Candurra, N. A. and Damonte, E. B. (1999). Myristic acid analogs are inhibitors of Junin virus replication. *Microbes Infect.* 1, 609-614. doi:10.1016/ S1286-4579(99)80060-4
- Cordo, S. M., Valko, A., Martinez, G. M. and Candurra, N. A. (2013). Membrane localization of Junín virus glycoproteins requires cholesterol and cholesterol rich membranes. *Biochem. Biophys. Res. Commun.* 430, 912-917. doi:10.1016/j.bbrc. 2012 12 053
- Enría, D. A., Mills, J. N., Bausch, D., Shieh, W. J. and Peters, C. J. (2011).
 Arenavirus infections. In: *Tropical Infectious Diseases: Principles, Pathogens, and Practice* (ed. R. L. Guerrant, D. H. Walker, and P. F. Weller), pp. 449-461. Elsevier.
- Episcopio, D., Aminov, S., Benjamin, S., Germain, G., Datan, E., Landazuri, J., Lockshin, R. A. and Zakeri, Z. (2019). Atorvastatin restricts the ability of influenza virus to generate lipid droplets and severely suppresses the replication of the virus. *FASEB J.* 33, 9516-9525. doi:10.1096/fj.201900428RR
- Farley, S. E., Kyle, J. E., Leier, H. C., Bramer, L. M., Weinstein, J. B., Bates, T. A., Lee, J.-Y., Metz, T. O., Schultz, C. and Tafesse, F. G. (2022). A global lipid map reveals host dependency factors conserved across SARS-CoV-2 variants. *Nat. Commun.* 13, 3487. doi:10.1038/s41467-022-31097-7
- Fujimoto, T. and Parton, R. G. (2011). Not just fat: The structure and function of the lipid droplet. *Cold Spring Harbor Perspect. Biol.* **3**, a004838. doi:10.1101/cshperspect.a004838
- García, C. C., Vázquez, C. A., Giovannoni, F., Russo, C. A., Cordo, S. M., Alaimo, A. and Damonte, E. B. (2020). Cellular organelles reorganization during Zika virus infection of human cells. *Front. Microbiol.* 11, 1558. doi:10.3389/fmicb. 2020.01558
- Gaudin, R. and Barteneva, N. S. (2015). Sorting of small infectious virus particles by flow virometry reveals distinct infectivity profiles. *Nat. Commun.* 6, 6022. doi:10. 1038/ncomms7022

- Gomes Dias, S. S., Cardoso Soares, V., Ferreira, A. C., Sacramento, C. Q., Fintelman-Rodrigues, N., Temerozo, J. R., Teixeira, L., Nunes Da Silva, M. A., Barreto, E., Mattos, M. et al. (2020). Lipid droplets fuel SARS-CoV-2 replication and production of inflammatory mediators. *PLoS Pathog.* 16, e1009127. doi:10. 1371/journal.ppat.1009127
- Gomes Dias, S. S., Cunha-Fernandes, T., Souza-Moreira, L., Cardoso Soares, V., Barbosa Lima, G., Azevedo-Quintanilha, I. G., Santos, J., Pereira-Dutra, F., Freitas, C., Reis, P. A. et al. (2023). Metabolic reprogramming and lipid droplets are involved in Zika virus replication in neural cells. *J. Neuroinflammation* 20, 61. doi:10.1186/s12974-023-02736-7
- Harris, C., Herker, E., Farese, R. V., Jr. and Ott, M. (2011). Hepatitis C virus core protein decreases lipid droplet turnover: A mechanism for core-induced steatosis. J. Biol. Chem. 286, 42615-42625. doi:10.1074/jbc.M111.285148
- Heaton, N. S. and Randall, G. (2010). Dengue virus-induced autophagy regulates lipid metabolism. *Cell Host Microbe* 8, 422-432. doi:10.1016/j.chom. 2010.10.006
- **Iqbal, J., Sarkar-Dutta, M., McRae, S., Ramachandran, A., Kumar, B. and Waris, G.** (2018). Osteopontin regulates Hepatitis C virus (HCV) replication and assembly by interacting with HCV proteins and lipid droplets and by binding to receptors αVβ3 and CD44. *J. Virol.* **92.** e02116-17. doi:10.1128/JVI.02116-17
- Itabe, H., Yamaguchi, T., Nimura, S. and Sasabe, N. (2017). Perilipins: a diversity of intracellular lipid droplet proteins. *Lipids Health Dis.* 16, 83. doi:10.1186/ s12944-017-0473-y
- Jordan, T. X. and Randall, G. (2017). Dengue virus activates the AMP kinasemTOR axis to stimulate a proviral lipophagy. *J. Virol.* 91, e02020-16. doi:10.1128/ ivi.02020-16
- Kimmel, A., Brasaemle, D., McAndrews-Hill, M., Sztalryd, C. and Londos, C. (2010). Adoption of PERILIPIN as a unifying nomenclature for the mammalian PAT-family of intracellular lipid storage droplet proteins. *J Lipid Res.* 51, 468-471. doi:10.1194/iir.R000034
- Kloska, A., Wesierska, M., Malinowska, M., Gabig- Ciminska, M. and Jakóbkiewicz-Banecka, J. (2020). Lipophagy and lipolysis status in lipid storage and lipid metabolism diseases. *Int. J. Mol. Sci.* 21, 1-33. doi:10.3390/ijms21176113
- Kumar, S., Yadav, D., Singh, D., Shakya, K., Rathi, B. and Poonam (2023). Recent developments on Junin virus, a causative agent for Argentine haemorrhagic fever. Rev. Med. Virol. 33, e2419. doi:10.1002/rmv.2419. Epub 2023 Jan 12.
- Loftus, T. M., Jaworsky, D. E., Frehywot, G. L., Townsend, C. A., Ronnett, G. V., Lane, M. D. and Kuhajda, F. P. (2000). Reduced food intake and body weight in mice treated with fatty acid synthase inhibitors. *Science* 288, 2379-2381. doi:10. 1126/science.288.5475.2379
- Manokaran, G., Flores, H. A., Dickson, C. T., Narayana, V. K., Kanojia, K., Dayalan, S., Tull, D., Mcconville, M. J., Mackenzie, J. M. and Simmons, C. P. (2020). Modulation of acyl-carnitines, the broad mechanism behind Wolbachia -mediated inhibition of medically important flaviviruses in Aedes aegypti. *Proc. Natl. Acad. Sci. USA* 117, 24475-24483. doi:10.1073/pnas.1914814117
- Mauthe, M., Orhon, I., Rocchi, C., Zhou, X., Luhr, M., Hijlkema, K. J., Coppes, R. P., Engedal, N., Mari, M. and Reggiori, F. (2018). Chloroquine inhibits autophagic flux by decreasing autophagosome-lysosome fusion. *Autophagy*. 14, 1435–1455. doi:10.1080/15548627.2018.1474314.
- Monson, E. A., Crosse, K. M., Duan, M., Chen, W., O'shea, R. D., Wakim, L. M., Carr, J. M., Whelan, D. R. and Helbig, K. J. (2021a). Intracellular lipid droplet accumulation occurs early following viral infection and is required for an efficient interferon response. *Nat. Commun.* 12, 4303. doi:10.1038/s41467-021-24632-5
- Monson, E. A., Trenerry, A. M., Laws, J. L., Mackenzie, J. M. and Helbig, K. J. (2021b). Lipid droplets and lipid mediators in viral infection and immunity. FEMS Microbiol. Rev. 45, 1-20. doi:10.1093/femsre/fuaa066
- Murphy, H. and Ly, H. (2022). Understanding immune responses to lassa virus infection and to its candidate vaccines'. Vaccines (Basel) 10, 1668. doi:10.3390/ vaccines10101668
- Olkkonen, V. M. and Hynynen, R. (2009). Interactions of oxysterols with membranes and proteins. *Mol. Asp. Med.* **30**, 123-133. doi:10.1016/j.mam. 2009.02.004
- Peña Cárcamo, J. R., Morell, M. L., Vázquez, C. A., Vatansever, S., Upadhyay, A. S., Överby, A. K., Cordo, S. M. and García, C. C. (2018). The interplay between viperin antiviral activity, lipid droplets and Junín mammarenavirus multiplication. *Virology* 514, 216-229. doi:10.1016/j.virol.2017.10.012
- Perez Vidakovics, M. L., Ure, A. E., Arrías, P. N., Romanowski, V. and Gómez, R. M. (2019). Junín virus induces autophagy in human A549 cells. *PLoS One* 14, e0218730. doi:10.1371/journal.pone.0218730
- Qu, Y., Wang, X., Zhu, Y., Wang, W., Wang, Y., Hu, G., Liu, C., Li, J., Ren, S., Xiao, M. Z. X. et al. (2021). ORF3a-mediated incomplete autophagy facilitates severe acute respiratory syndrome coronavirus-2 replication. Front. Cell Dev. Biol. 9, 716208. doi:10.3389/fcell.2021.716208
- Radoshitzky, S. R. and de la Torre, J. C. (2019). Human Pathogenic Arenaviruses (Arenaviridae). In *Encyclopedia of Virology (Fourth Edition)*, (eds. D. H. Bamford and M. Zuckerman), pp. 507-517. Academic Press. doi:10.1016/B978-0-12-814515-9.00014-X
- Rentero, C., Zech, T., Quinn, C. M., Engelhardt, K., Williamson, D., Grewal, T., Jessup, W., Harder, T. and Gaus, K. (2008). Functional implications of plasma

- membrane condensation for T cell activation. *PLoS One* **3**, e2262. doi:10.1371/journal.pone.0002262
- Roldán, J. S., Candurra, N. A., Colombo, M. I. and Delgui, L. R. (2019). Junín virus promotes autophagy to facilitate the virus life cycle. *J. Virol.* 93, e02307-18. doi:10.1128/jvi.02307-18
- Samsa, M. M., Mondotte, J. A., Iglesias, N. G., Assunco-Miranda, I., Barbosa-Lima, G., Da Poian, A. T., Bozza, P. T. and Gamarnik, A. V. (2009). Dengue virus capsid protein usurps lipid droplets for viral particle formation. *PLoS Pathog.* 5, e1000632. doi:10.1371/journal.ppat.1000632
- Schindelin, J., Arganda-Carreras, I., Frise, E., Kaynig, V., Longair, M., Pietzsch, T., Preibisch, S., Rueden, C., Saalfeld, S., Schmid, B. et al. (2012). Fiji: an open-source platform for biological-image analysis. *Nat. Methods* 9, 676-682. doi:10.1038/nmeth.2019
- Schulze, R. J., Krueger, E. W., Weller, S. G., Johnson, K. M., Casey, C. A., Schott, M. B. and Mcniven, M. A. (2020). Direct lysosome-based autophagy of lipid droplets in hepatocytes. *Proc. Natl. Acad. Sci. U.S.A.* 117, 32443-32452. doi:10.1073/PNAS.2011442117
- Sepúlveda, C. S., Cordo, S. M., Vázquez, C. A., García, C. C. and Damonte, E. B. (2022). Arenaviruses. In *Encyclopedia of Infection and Immunity* (ed N. Rezaei), pp. 278-291. Elsevier. doi:10.1016/B978-0-12-818731-9.00031-8
- Shao, J., Huang, Q., Liu, X., Di, D., Liang, Y. and Ly, H. (2018). Arenaviral nucleoproteins suppress PACT-induced augmentation of RIG-I function to inhibit type i interferon production. J. Virol. 92, e00482-18. doi:10.1128/JVI.00482-18
- Singh, R. and Cuervo, A. M. (2012). Lipophagy: connecting autophagy and lipid metabolism. *Int. J. Cell Biol.* 2012, 282041. doi:10.1155/2012/282041
- Stoyanova, G., Jabeen, S., Landazuri Vinueza, J., Ghosh Roy, S., Lockshin, R. A. and Zakeri, K. (2023). Zika Virus triggers autophagy to exploit host lipid metabolism and drive viral replication. *Cell Commun. Signal.* 21, 114. doi:10.1186/s12964-022-01026-8
- Sun, L. J., Li, S. C., Zhao, Y. H., Yu, J. W., Kang, P. and Yan, B. Z. (2013). Silent information regulator 1 inhibition induces lipid metabolism disorders of hepatocytes and enhances hepatitis C virus replication. *Hepatol. Res.* 43, 1343-1351. doi:10.1111/hepr.12089
- Teixeira, L., Pereira-Dutra, F. S., Reis, P. A., Cunha-Fernandes, T., Yoshinaga, M. Y., Souza-Moreira, L., Souza, E. K., Barreto, E. A., Silva, T. P. and Espinheira-Silva, H. et al. (2024). Prevention of lipid droplet accumulation by

- DGAT1 inhibition ameliorates sepsis-induced liver injury and inflammation. *JHEP Rep.* **6**, 100984. doi:10.1016/j.jhepr.2023.100984
- Veliziotis, I., Roman, A., Martiny, D., Schuldt, G., Claus, M., Dauby, N., Van Den Wijngaert, S., Martin, C., Nasreddine, R., Perandones, C. et al. (2020). Clinical management of argentine hemorrhagic fever using Ribavirin and Favipiravir, Belgium, 2020. Emerg. Infect. Dis. 26, 1562-1566. doi:10.3201/EID2607.200275
- Vieyres, G., Reichert, I., Carpentier, A., Vondran, F. W. R. and Pietschmann, T. (2020). The ATGL lipase cooperates with ABHD5 to mobilize lipids for hepatitis C virus assembly. *PLoS Pathog.* **16**, e1008554. doi:10.1371/journal.ppat.1008554
- Viktorova, E. G., Nchoutmboube, J. A., Ford-Siltz, L. A., Iverson, E. and Belov, G. A. (2018). Phospholipid synthesis fueled by lipid droplets drives the structural development of poliovirus replication organelles. *PLoS Pathog.* 14, e1007280. doi:10.1371/journal.ppat.1007280
- Wang, H. Q., Altomare, D. A., Skele, K. L., Poulikakos, P. I., Kuhajda, F. P., Di Cristofano, A. and Testa, J. R. (2005). Positive feedback regulation between AKT activation and fatty acid synthase expression in ovarian carcinoma cells. *Oncogene* 24, 3574-3582. doi:10.1038/sj.onc.1208463
- Wang, W., Qu, Y., Wang, X., Xiao, M. Z. X., Fu, J., Chen, L., Zheng, Y. and Liang, Q. (2023). Genetic variety of ORF3a shapes SARS-CoV-2 fitness through modulation of lipid droplet. J. Med. Virol. 95, e28630. doi:10.1002/jmv.28630
- Wolff, S., Becker, S. and Groseth, A. (2013). Cleavage of the Junin virus nucleoprotein serves a decoy function to inhibit the induction of apoptosis during infection. J. Virol. 87, 224-233. doi:10.1128/jvi.01929-12
- York, J. and Nunberg, J. H. (2016). Myristoylation of the arenavirus envelope glycoprotein stable signal peptide is critical for membrane fusion but dispensable for virion morphogenesis. J. Virol. 90, 8341-8350. doi:10.1128/jvi. 01124-16
- Zhang, J., Lan, Y. and Sanyal, S. (2017). Modulation of lipid droplet metabolism-a potential target for therapeutic intervention in *Flaviviridae* infections. *Front. Microbiol.* 8, 2286. doi:10.3389/fmicb.2017.02286
- Zhang, J., Lan, Y., Li, M. Y., Lamers, M. M., Fusade-Boyer, M., Klemm, E., Thiele, C., Ashour, J. and Sanyal, S. (2018). Flaviviruses exploit the lipid droplet protein AUP1 to trigger lipophagy and drive virus production. *Cell Host Microbe* 23, 819-831.e5. doi:10.1016/j.chom.2018.05.005
- Zheng, Q., Huang, Y., Wang, L., Zhang, Y., Guo, X., Huang, X. and Qin, Q. (2022).
 SGIV induced and exploited cellular De Novo fatty acid synthesis for virus entry and replication. Viruses 14, 180. doi:10.3390/v14020180

 Table S1. Primer sequences for RT-PCR.

Gene name	Protein	Primers
n	JUNV NP protein	5'-CGCACAGTGGATCCTAGGC-3'
		5'-GGCATCCTTCAGAACATC-3'
Z	JUNV Z protein	5'-ATGGGCAACTGCAACGGGGCATC-3'
		5'-CTATGGTTGGTGGTGCTGTTGGCT-3
ACTB	β-actin	5'-GAGACCTTCAACACCCCAGCC-3'
		5'-GGCCATCTCTTGCTCGAAGTC-3'
PLIN2	Perilipin 2	5'-CTGATGAGTCCCACTGTGCTGA-3'
		5'-TGTGGCACGTGGTCTGGAG-3'
FASN	Fatty acid synthase	5'-AAGGACCTGTCTAGGTTTGATGC-3'
		5'-TGGCTTCATAGGTGACTTCCA-3'
DGAT1	Diacylglycerol O- Acyltransferase 1	5'-TATTGCGGCCAATGTCTTTGC-3'
	7 toyliransierase 1	5'-CACTGGAGTGATAGACTCAACCA-3'
DGAT2	Diacylglycerol O- Acyltransferase 2	5'-AGTGGCAATGCTATCATCAT-3'
	Acyttatisiciase 2	5'-GAGGCCTCGACCATGGAAGAT-3'
PNPLA2	Adipose Triglyceride Lipase	5'-ACCAGCATCCAGTTCAACCT-3'
		5'-ATCCCTGCTTGCACATCTCT-3'
CPT1A	Carnitine Palmitoyltransferase 1A	5'-ACAGTCGGTGAGGCCTCTTA-3'
	T aminoyinansierase IA	5'-CCACCAGTCGCTCACGTAAT-3'